Electronic Supplementary Material (ESI) for Inorganic Chemistry Frontiers.

SUPPORTING INFORMATION

Colloidal suspensions of highly luminescent lanthanide-based coordination polymers molecular alloys for ink-jet printing and tagging of technical liquids.

Youenn Pointel[a,b,c], Carole Daiguebonne[a,c], Yan Suffren[a,c,*], Francois Le Natur[b,c], Stéphane Freslon[a,c], Guillaume Calvez[a,c], Kevin Bernot[a,c,d], David Jacob[e] and Olivier Guillou[a,c].

[a] Univ Rennes, INSA Rennes, CNRS UMR 6226 "Institut des Sciences Chimiques de Rennes", F-35708 Rennes, France.

[b] Olnica, 40 Rue du Bignon, F-35135 Chantepie, France.

[c] ChemInTag, INSA Rennes, Olnica, F-35708 Rennes, France.

[d] Institut Universitaire de France (IUF) 1 rue Descartes, F-75231 Paris, France.

[e] Cordouan Technologies, Cité de la photonique, Bat Pleione, 11 Avenue de Canteranne, 33600 PESSAC, France.

* To whom correspondence should be addressed: Yan.Suffren@insa-rennes.fr

X-ray powder diffraction.

Iso-structurality of the prepared molecular alloys, with $[Eu_2(dcpa)_3(H_2O)]_\infty$[1] was assumed on the basis of their X-ray powder diffraction diagrams. Diagrams were collected using a Panalytical X'Pert Pro diffractometer equipped with an X'Celerator detector. Recording conditions were: 45 kV, 40 mA for Cu Kα (λ = 1.542 Å) in θ/θ mode between 5° and 75°. Calculated patterns were produced using PowderCell and WinPLOTR programs.[2-4]

Electron Dispersive Spectroscopy.

Relative metallic contents of the different microcrystalline powders have been estimated on the basis of ESD measurements. EDS measurements have been performed with a Hitachi TM-1000, Tabletop Microscope version 02.11 (Hitachi High-Technologies, Corporation Tokyo Japan) with EDS analysis system (SwiftED-TM, Oxford Instruments Link INCA). Samples were deposited on carbon discs. Reproducibility of the elemental analyses has been checked by repeating the measurements several times. These experiments confirm the homogeneity of the samples.

Optical measurements

Solid-state/colloidal suspensions emission and excitation spectra have been measured on a Horiba Jobin-Yvon Fluorolog III fluorescence spectrometer equipped with a Xe lamp 450 W, a UV-Vis photomultiplier (Hamamatsu R928, sensitivity 190-860 nm) and an IR-photodiode cooled by liquid nitrogen (InGaAs, sensitivity 800-1600 nm) or on a Horiba Jobin-Yvon FluoroMax 4 Plus fluorescence spectrometer equipped with a Xe lamp 150 W and a UV-Vis photomultiplier (Hamamatsu R928, sensitivity 190-860 nm). Quantum yield measurements were performed using F-3018 Jobin-Yvon or G8 GMP integrating spheres ($\Phi = (E_c - E_a)/(L_a - L_c)$ with E_c being the integrated emission spectrum of the sample, E_a the

integrated “blank” emission spectrum, L_a the “blank” absorption and L_c the sample absorption at the excitation wavelength). Solid-state and colloidal suspensions emission/excitation spectra were realized directly on powder samples shaped into pellets or on suspensions placed inside an emission cuvette. For the quantum yield recordings of, the powder or the dispersion samples are introduced in cylindrical quartz cells of 0.7 cm diameter and 2.4 cm height (F-3018) or in small capillaries (G8), which were placed directly inside the integrating spheres. For the measurements realized at variable temperature (77 K – 363 K), the samples were introduced in an OptistatCF liquid nitrogen cooled cryostat (77 K – 300 K) from Oxford Instruments and in a Peltier heating module (300 K – 363 K) from Horiba Jobin-Yvon. Longest luminescence decays ($\tau > 10$ µs) have also been measured at room-temperature using this apparatus with a Xenon flash lamp (phosphorescence mode) on the Fluorolog. Lifetimes and quantum yields are averages of two or three independent determinations.

Comparative luminescent spectra have been measured on the same fluorimeter on powder samples shaped into pellets or colloidal suspensions introduced inside an emission cuvette. Spectra were recorded under identical operating conditions and without turning the lamp off to ensure a valid comparison between the emission spectra.

Appropriate filters were used to remove the residual excitation laser light, the Rayleigh scattered light and associated harmonics from spectra. All spectra were corrected for the instrumental response function.

Luminance of the samples expressed in $cd.m^{-2}$ have been measured with a Gigahertz-Optik X1-1 optometer with an integration time of 200 ms on 1.5 cm^2 pellets under UV irradiation ($\lambda_{exc} = 312$ nm). The intensity of the UV flux at sample location, 0.75(2) $mW.cm^{-2}$, has been measured with a VilberLourmat VLX-3W radiometer. $[Tb_2(bdc)_3 \cdot 4H_2O]_\infty$ where bdc^{2-} stands for terephthalate was used as a standard. Its luminance is 136(4) $cd.m^{-2}$ under these operating conditions ($\lambda_{exc} = 312$ nm; flux = 0.75(2) $mW.cm^{-2}$).[5]

The CIE (Commission Internationale de l'Eclairage) (x, y) emission color coordinates[6-7] were measured with a MSU-003 colorimeter (Majantys) equipped with the PhotonProbe 1.6.0 Software (Majantys). Color measurements: 2°, CIE 1931, step 5 nm, under 312 nm UV light. $X = k \times \int_{380nm}^{780nm} I_\lambda \times x_\lambda$, $Y = k \times \int_{380nm}^{780nm} I_\lambda \times y_\lambda$ and $Z = k \times \int_{380nm}^{780nm} I_\lambda \times z_\lambda$ with k constant for the measurement system, I_λ sample spectrum intensity wavelength depending, x_λ, y_λ, z_λ trichromatic values x = X/(X+Y+Z), y = Y/(X+Y+Z) and z = Z/(X+Y+Z). Mean xyz values are given for each sample, which act as light sources (luminescent samples). Standards from Phosphor Technology used, calibrated at 312 nm: red phosphor Gd_2O_2S:Eu (x = 0.667, y = 0.330) and green phosphor Gd_2O_2S:Tb (x = 0.328, y = 0.537).

Table S1. Relative metallic contents measured by EDS of $[Eu_{0.2}La_{1.8}(dcpa)_3(H_2O)]_\infty$.				
	Expected ratio (%)		Experimental ratio (%)	
$[Eu_{0.2}La_{1.8}(dcpa)_3(H_2O)]_\infty$	La (III)	Eu (III)	La (III)	Eu (III)
	90	10	91(2)	9(2)

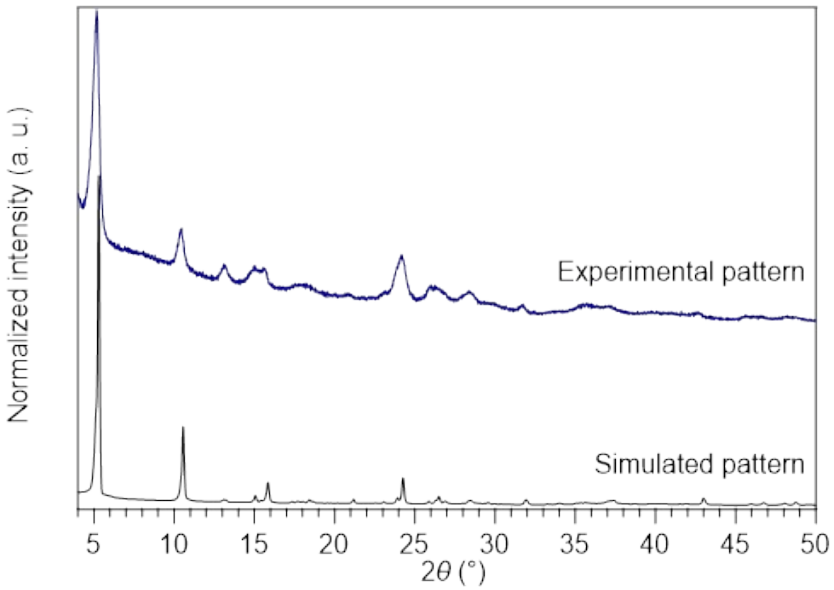

Figure S1. Experimental powder X-ray diffraction pattern of $[Eu_{0.2}La_{1.8}(dcpa)_3(H_2O)]_\infty$ and simulated X-ray powder diffraction diagram of $[Eu_2(dcpa)_3(H_2O)]_\infty$ on the basis of its crystal structure.

Table S2. Relative metallic contents measured by EDS of $[Tb_{0.2}La_{1.8}(dcpa)_3(H_2O)]_\infty$.				
	Expected ratio (%)		Experimental ratio (%)	
$[Tb_{0.2}La_{1.8}(dcpa)_3(H_2O)]_\infty$	La (III)	Tb (III)	La (III)	Tb (III)
	90	10	89(2)	11(2)

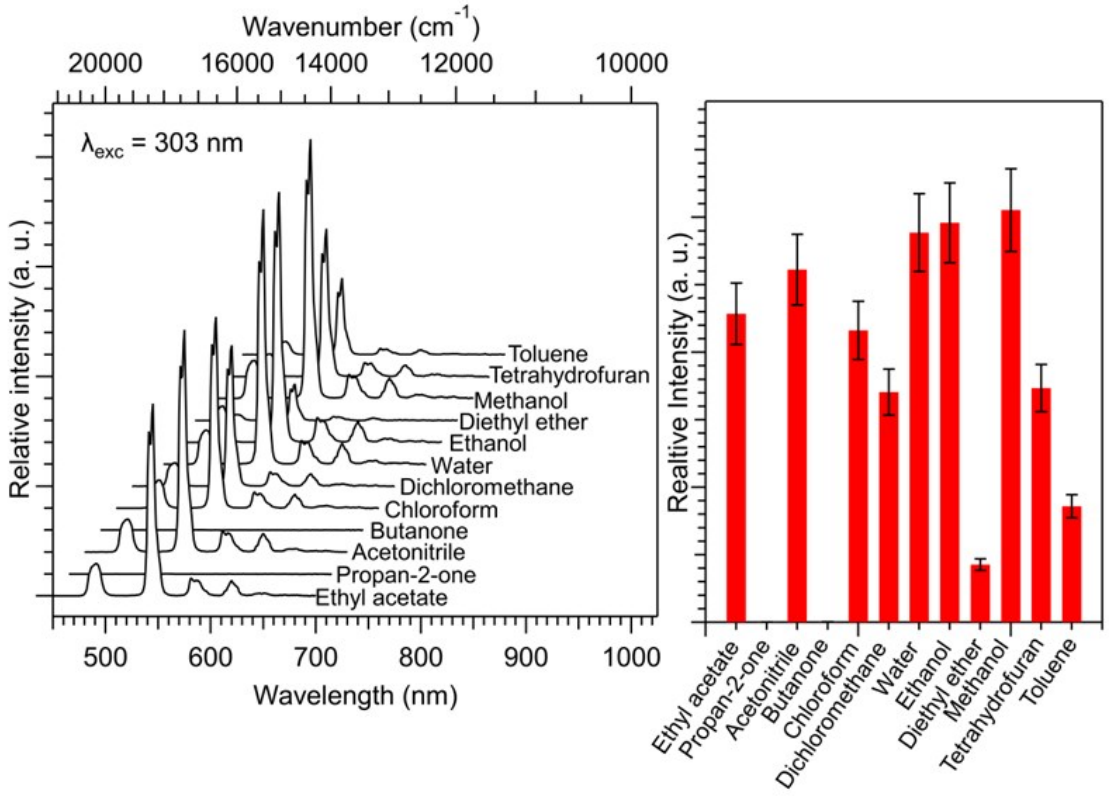

Figure S2. Emission spectra (λ_{exc} = 303 nm) of the colloidal suspensions of $[Tb_{0.2}La_{1.8}(dcpa)_3(H_2O)]_\infty$ in various solvent (left) and integrated area of the characteristic emission peaks of Tb^{3+} ions after 2 days (right), error bars = 10%.

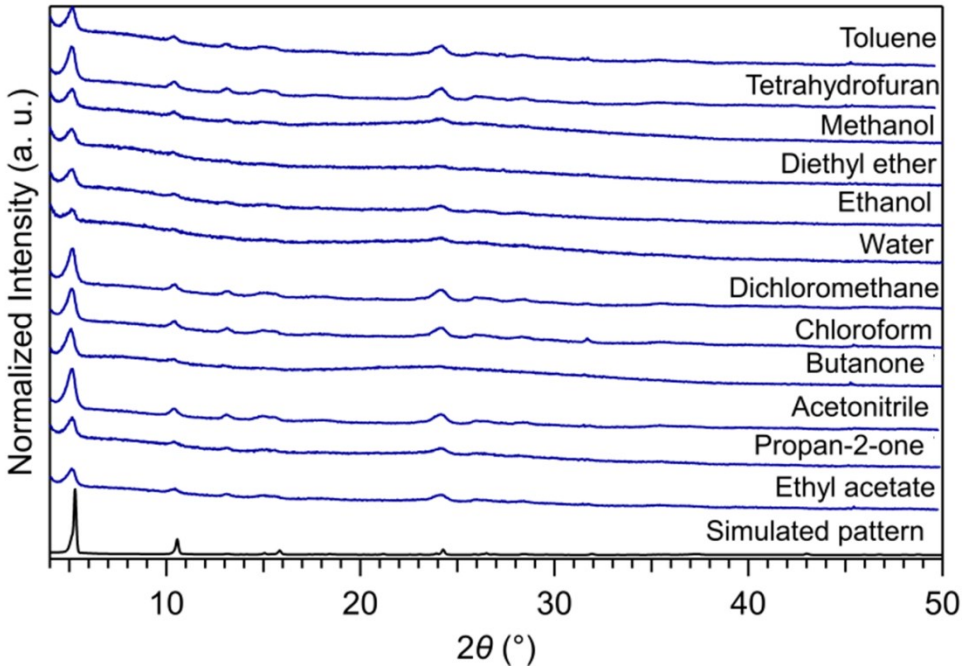

Figure S3. Experimental powder X-ray diffraction patterns of the solids obtained after evaporation of the solvents of the colloidal suspensions of $[Tb_{0.2}La_{1.8}(dcpa)_3(H_2O)]_\infty$ and simulated powder X-ray diffraction diagram of $[Eu_2(dcpa)_3(H_2O)]_\infty$.

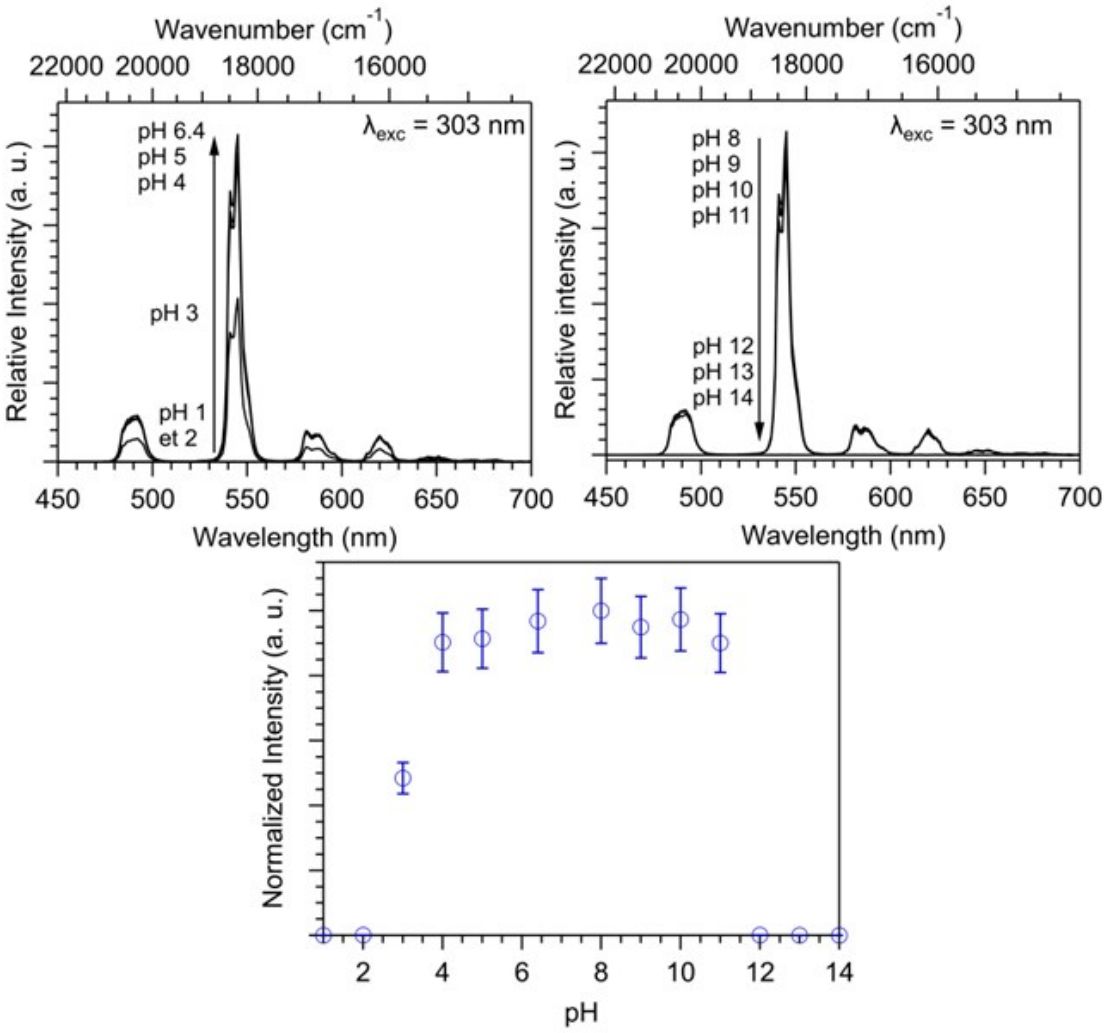

Figure S4. Emission spectra ($\lambda_{exc} = 303$ nm) of the aqueous colloidal suspensions of $[Tb_{0.2}La_{1.8}(dcpa)_3(H_2O)]_\infty$ in water *vs* pH (top) and integrated area of the characteristic emission peaks of Tb^{3+} ions (bottom), error bars = 10%.

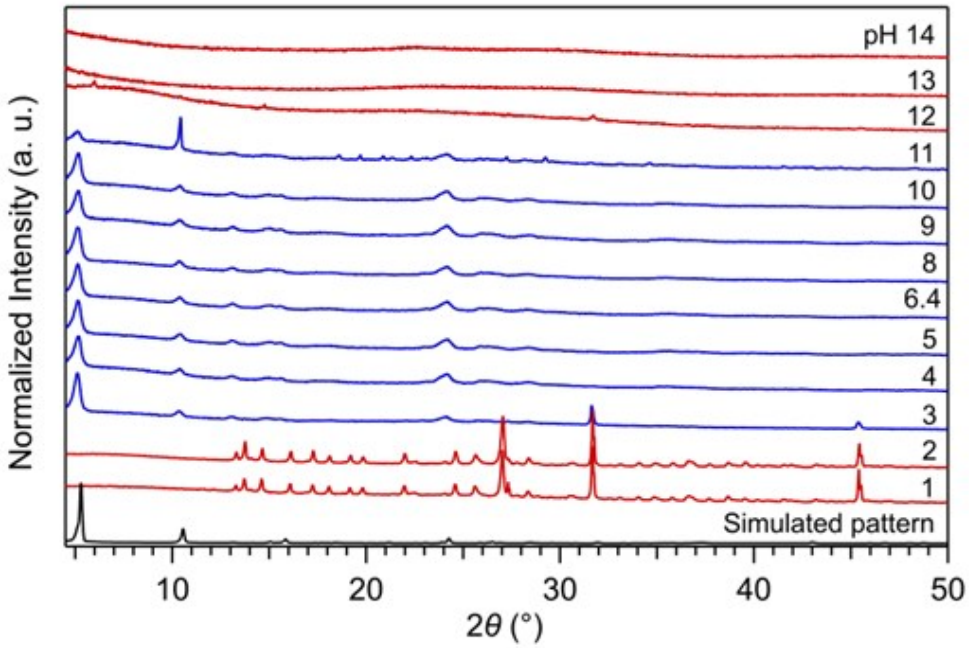

Figure S5. Experimental powder X-ray diffraction patterns of the solids obtained after evaporation of the water of the colloidal suspensions of $[Tb_{0.2}La_{1.8}(dcpa)_3(H_2O)]_\infty$ *vs* pH and simulated powder X-ray diffraction diagram of $[Eu_2(dcpa)_3(H_2O)]_\infty$.

Table S3. Relative metallic contents measured by EDS of $[TbLa(dcpa)_3(H_2O)]_\infty$ ❶, $[EuLa(dcpa)_3(H_2O)]_\infty$ ❷ and $[Eu_{0.5}Tb_{0.5}La(dcpa)_3(H_2O)]_\infty$ ❹.

	Expected ratio (%)			Experimental ratio (%)		
	La (III)	Eu (III)	Tb (III)	La (III)	Eu (III)	Tb (III)
❶	50	-	50	47(3)	-	53(3)
❷	50	50	-	48(3)	52(3)	-
❹	50	25	25	47(3)	27(3)	26(3)

Table S4. Relative metallic contents measured by EDS of $[Sm_{0.2}La_{1.8}(dcpa)_3(H_2O)]_\infty$, $[Eu_{0.2}La_{1.8}(dcpa)_3(H_2O)]_\infty$, $[Tb_{0.2}La_{1.8}(dcpa)_3(H_2O)]_\infty$ and $[Dy_{0.2}La_{1.8}(dcpa)_3(H_2O)]_\infty$.

	Expected ratio (%)		Experimental ratio (%)	
$[Sm_{0.2}La_{1.8}(dcpa)_3(H_2O)]_\infty$	La (III) 90	Sm (III) 10	La (III) 91(2)	Sm (III) 9(2)
$[Eu_{0.2}La_{1.8}(dcpa)_3(H_2O)]_\infty$	La (III) 90	Eu (III) 10	La (III) 91(2)	Eu (III) 9(2)
$[Tb_{0.2}La_{1.8}(dcpa)_3(H_2O)]_\infty$	La (III) 90	Tb (III) 10	La (III) 89(2)	Tb (III) 11(2)
$[Dy_{0.2}La_{1.8}(dcpa)_3(H_2O)]_\infty$	La (III) 90	Dy (III) 10	La (III) 90(2)	Dy (III) 10(2)

Table S5. Relative metallic contents measured by EDS of $[Eu_{0.2x}Tb_{0.2-0.2x}La_{1.8}(dcpa)_3(H_2O)]_\infty$ with $0 \leq x \leq 1$.

x	Expected ratio (%)			Experimental ratio (%)		
	La (III)	Eu (III)	Tb (III)	La (III)	Eu (III)	Tb (III)
0	90	0	10	90(2)	-	10(2)
0.1	90	1	9	90(2)	1(3)	9(2)
0.2	90	2	8	89(3)	2(2)	8(3)
0.3	90	3	7	89(2)	3(1)	7(1)
0.4	90	4	6	90(2)	4(2)	6(1)
0.5	90	5	5	89(3)	5(3)	6(2)
0.6	90	6	4	90(2)	6(1)	4(2)
0.7	90	7	3	90(2)	7(2)	3(2)
0.8	90	8	2	90(3)	8(3)	2(2)
0.9	90	9	1	89(2)	10(2)	1(3)
1	90	10	0	90(2)	10(2)	-

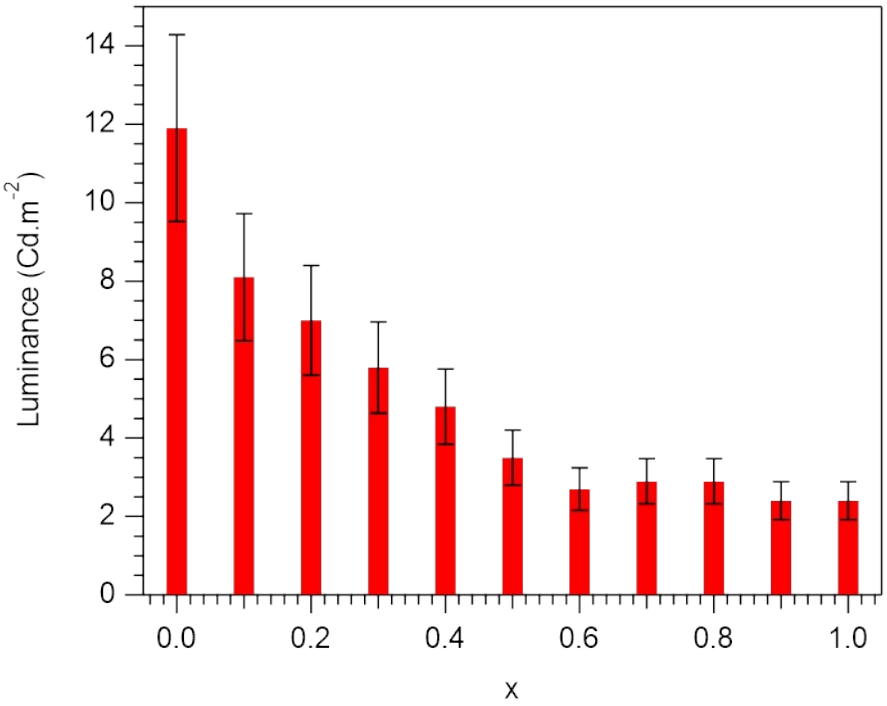

Figure S6. Luminance *versus* x of colloidal suspensions of $[Eu_{0.2x}Tb_{0.2-0.2x}La_{1.8}(dcpa)_3(H_2O)]_\infty$:EtOH (0.3 g.L^{-1}) with $0 \leq x \leq 1$ under 312 nm excitation wavelength (Flux = 0.75(2) mW.m^{-2}), error bars = 20%.

Table S6. Relative metallic contents measured by EDS of $[Sm_{0.07}Eu_{0.02}Tb_{0.04}Dy_{0.07}La_{1.8}(dcpa)_3(H_2O)]_\infty$.

Expected ratio (%)					Experimental ratio (%)				
La(III)	Sm(III)	Eu(III)	Tb(III)	Dy(III)	La(III)	Sm(III)	Eu(III)	Tb(III)	Dy(III)
90	3.5	1	2	3.5	90(2)	5(2)	1(1)	1(2)	3(2)

Table S7. Relative metallic contents measured by EDS of $[Tb_{0.16}Eu_{0.04}La_{1.8}(dcpa)_3(H_2O)]_\infty$.

Expected ratio (%)			Experimental ratio (%)		
La (III)	Eu (III)	Tb (III)	La (III)	Eu (III)	Tb (III)
90	2	8	89(2)	2(1)	8(1)

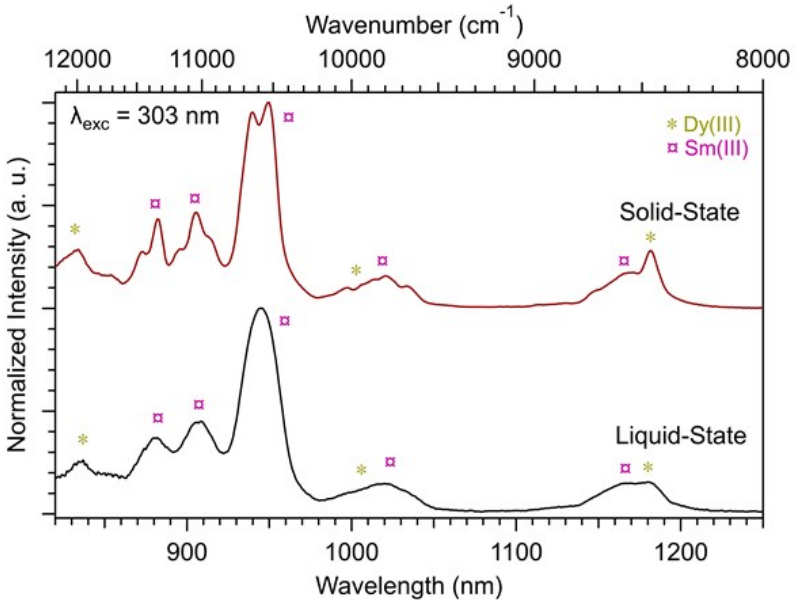

Figure S7. Emission spectra (λ_{exc} = 303 nm) of $[Sm_{0.07}Eu_{0.02}Tb_{0.04}Dy_{0.07}La_{1.8}(dcpa)_3(H_2O)]_\infty$ and $[Sm_{0.07}Eu_{0.02}Tb_{0.04}Dy_{0.07}La_{1.8}(dcpa)_3(H_2O)]_\infty$:EtOH (0.3 g.L^{-1}) in the IR domain.

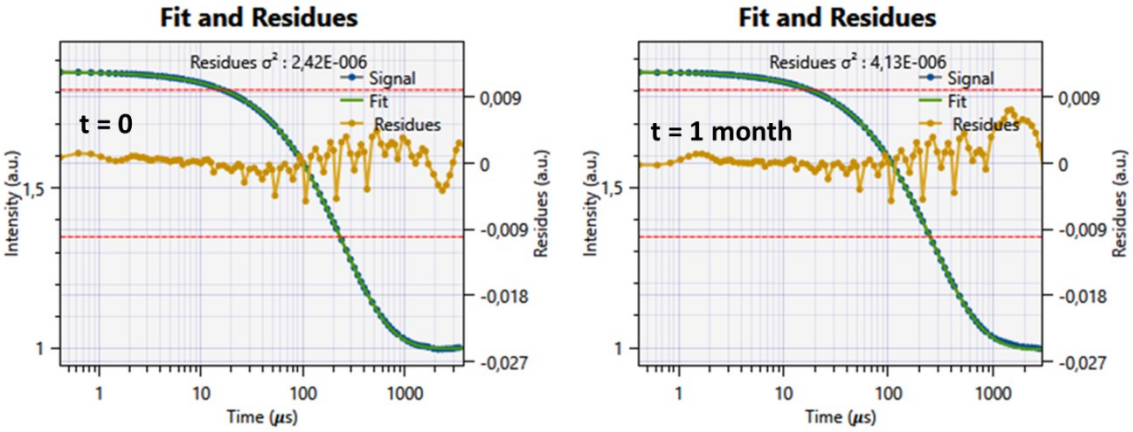

Figure S8. Best autocorrelation fits of the DLS measurements for $[Eu_{0.2}La_{1.8}(dcpa)_3(H_2O)]_\infty$:EtOH (0.3 g.L^{-1}) at t = 0 and t = 1 month with Cumulants algorithm.

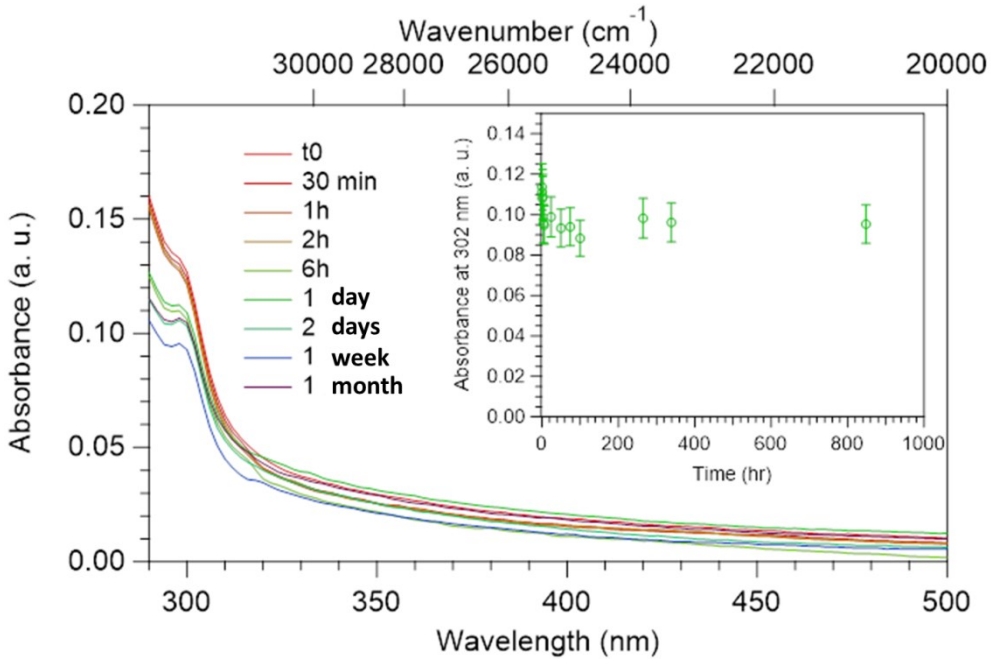

Figure S9. Absorbance *versus* time of colloidal suspensions of $[Eu_{0.2}La_{1.8}(dcpa)_3(H_2O)]_\infty$:EtOH (0.3 $g.L^{-1}$) between 290 and 500 nm. In inset: absorbance at 303 nm *versus* time, error bars = 10%.

REFERENCES.

1. He, H.; Chen, S.-H.; Zhang, D.-Y.; Hao, R.; Zhang, C.; Yang, E.-C.; Zhao, X.-J., A micrometer-sized europium(III)–organic framework for selective sensing of the $Cr2O7^{2-}$ anion and picric acid in water systems. *Dalton Trans.* **2017,** *46*, 13502-13509.
2. Kraus, W.; Nolze, G., POWDER CELL - A program for the representation and manipulation of crystal structures and calculation of the resulting X-ray powder patterns. *J. Appl. Crystallogr.* **1996,** *29*, 301-303.
3. Roisnel, T.; Rodriguez-Carjaval, J., A Window Tool for Powder Diffraction Patterns Analysis. *J. Mater. Sci. Forum* **2001,** *378*, 118-123.
4. Roisnel, T.; Rodriguez-Carjaval, J., WinPLOTR : a windows tool for powder diffraction pattern analysis. *Materials Science Forum, Proceedings of the Seventh European Powder Diffraction Conference (EPDIC 7)* **2000**, 118-123.
5. Haquin, V.; Etienne, M.; Daiguebonne, C.; Freslon, S.; Calvez, G.; Bernot, K.; Le Polles, L.; Ashbrook, S. E.; Mitchell, M. R.; Bünzli, J. C. G.; Guillou, O., Color and brightness tuning in hetero-nuclear lanthanide teraphthalate coordination polymers. *Eur. J. Inorg. Chem.* **2013**, 3464-3476.
6. CIE, *International Commission on Illumination - Technical report*. CIE: **1995;** Vol. 13-3, p 16.
7. Wyszecki, G., Colorimetry. In *Handbook of Optics*, Driscoll, W. G.; Vaughan, W., Eds. Mac Graw-Hill Book Company: New-York, **1978**, p 1-15.